Talanta 88 (2012) 152–159

Contents lists available at SciVerse ScienceDirect

Talanta

journal homepage: www.elsevier.com/locate/talanta

Selective detection of carbon dioxide using LaOCl-functionalized SnO_2 nanowires for air-quality monitoring

Do Dang Trung[a], Le Duc Toan[a], Hoang Si Hong[b], Tran Dai Lam[c], Tran Trung[d,*], Nguyen Van Hieu[a,**]

[a] International Training Institute for Materials Science, Hanoi University of Science and Technology, No. 1, Dai Co Viet, Hanoi, Viet Nam
[b] School of Electrical Engineering, Hanoi University of Science and Technology, Hanoi, Viet Nam
[c] Institute of Materials Science, Vietnamese Academy of Science and Technology, Hanoi, Viet Nam
[d] Faculty of Environment and Chemistry, Hung Yen University of Technology and Education, Khoai Chau, Hung Yen, Viet Nam

ARTICLE INFO

Article history:
Received 26 July 2011
Received in revised form 15 October 2011
Accepted 20 October 2011
Available online 25 October 2011

Keywords:
SnO_2 nanowires
LaOCl
CO_2 sensor

ABSTRACT

In spite of the technical important of monitoring CO_2 gas by using a semiconductor-type gas sensor, a good sensitive and selective semiconductor CO_2 sensor has been not realized due to the rather unreactive toward CO_2 of conventional semiconductor metal oxides. In this work, a novel semiconductor CO_2 sensor was developed by functionalizing SnO_2 nanowires (NWs) with LaOCl, which was obtained by heat-treating the SnO_2 NWs coating with $LaCl_3$ aqueous solution at a temperature range of 500–700 °C. The bare SnO_2 NWs and LaOCl–SnO_2 NWs sensors were characterized with CO_2 (250–4000 ppm) and interference gases (100 ppm CO, 100 ppm H_2, 250 ppm LPG, 10 ppm NO_2 and 20 ppm NH_3) at different operating temperatures for comparison. The SnO_2 NWs sensors functionalized with different concentrations of $LaCl_3$ solution were also examined to find optimized values. Comparative gas sensing results reveal that LaOCl–SnO_2 NWs sensors exhibit much higher response, shorter response–recovery and better selectivity in detecting CO_2 gas at 400 °C operating temperature than the bare SnO_2 NWs sensors. This finding indicates that the functionalizing with LaOCl greatly improves the CO_2 response of SnO_2 NWs-based sensor, which is attributed to (i) p–n junction formation of LaOCl (p-type) and SnO_2 nanowires (n-type) that led to the extension of electron depletion and (ii) the favorable catalytic effect of LaOCl to CO_2 gas.

1. Introduction

The recent increase in the emission of carbon dioxide (CO_2) due to human activities has led to the considerable attention to CO_2 gas as a noxious substance and a global warming factor. Thus, the demand in detection of CO_2 gas has been increasing, particularly in controlling environmental condition, such as air-quality monitoring, fire detection, engine exhausts, agricultural development, bio-related and chemical processes [1,2]. Feasible and low-cost monitoring of CO_2 gas from low to high concentrations allow early detection of environmental hazards and provides time for an effective countermeasure [3]. Various types of CO_2 sensors such as infrared [4], solid electrolyte [5], capacitive [6], surface acoustic wave s [8], fluorescent chemo-sensors [9], and semiconductive metal oxide (SMO)-based sensors [10–17], have been demonstrated. Among of these sensing platforms, SMO sensors have important advantages, such as low cost, good reliability, small size, easy mass production, and potential development of array-integrated gas sensors [1]. For the past decades, much effort has been exerted to develop CO_2 gas sensors based on conventional SMO materials [10–17]. According to these reports, the sensitivity, selectivity, and response–recovery time of SMO-based sensors to CO_2 gas still need to be improved for particular applications.

SnO_2 nanowires (NWs) are among the most promising material systems for semiconductor gas sensors, with advantages, such as large surface-to-volume ratio, higher crystallinity, and better stoichiometric control [18]. The NWs sensors function by converting surface chemical processes, which are often catalytic processes into observable conductance variations in the NWs. Significant progress, including NWs surface functionalization [19,21], NWs doping [22], NWs core–shell [23], hierarchical NWs [24], on-chip grown NWs [25,26], wire-diameter control [27], and self-heating sensing [28], has been made to enhance the performance of SnO_2 NWs-based sensors. Among these methods, functionalizing NWs with catalytic nanoparticles is one of the most cost-effective and feasible methods enhancing sensitivity and selectivity to particular gases for SnO_2 NWs-based sensors [29]. In addition, this method would be very powerful to develop SnO_2 NWs multi-sensors for the

* Corresponding author. Tel.: +84 321 3713558; fax: +84 321 3713015.
** Corresponding author. Tel.: +84 4 38680787; fax: +84 4 38692963.
E-mail addresses: trantrung@utehy.edu.vn (T. Trung), hieu@itims.edu.vn (N. Van Hieu).

0039-9140/$ – see front matter © 2011 Elsevier B.V. All rights reserved.
doi:10.1016/j.talanta.2011.10.024

environmental monitoring by using an alternative catalyst coating. The multi-sensors is a technical important of environmental monitoring, because it can be used to detect a series of toxic gases, such as CO, CO_2, SO_2, NO_2, NO, N_2O, H_2S, hydrocarbons, VOCs (volatile organic compounds) [30]. SnO_2 NWs coated with Pd [19,31], La_2O_3 [21], Au [32], and CuO [33] for the corresponsive detection of H_2, C_2H_5OH, CO and H_2S gases with very good sensitivity and selectivity has been reported. However, the development of high performance CO_2 gas sensors remains a challenge for SnO_2 NWs. LaOCl is one of the most promising materials for sensitive and selective detection of CO_2 gas because of the favorable absorption of CO_2 on the LaOCl surface through the formation of a carbonate based on the lanthanum site [16]. In addition, LaOCl is a p-type semiconductor, used forming the p–n junction with n-type SnO_2 NWs to enhance the performance of the gas sensor [34]. Therefore, the present study proposes a simple and effective process to develop a CO_2 gas sensor with good sensitivity, selectivity and relatively short response–recovery time using the LaOCl-functionalized SnO_2 NWs (LaOCl–SnO_2 NWs). The mechanism which the CO_2 sensing properties of LaOCl–SnO_2 NWs are enhanced is also discussed.

2. Experimental

SnO_2 WNs were synthesized according to previous works [24,26]. The SnO_2 NWs were synthesized on Au-coated Si substrates through a simple thermal evaporation of Sn metal powders (99.9%). The source material was loaded in an alumina boat, placed at the center of a quartz tube in a horizontal-type furnace. The furnace was heated to 800 °C and kept for 30 min during the synthesis of the NWs. The pressure in the quartz tube was controlled at 5–10 Torr using O_2 gas with a flow rate of 0.4–0.5 sccm. The as-synthesized SnO_2 NWs were analyzed through field emission scanning electron microscopy (FE-SEM, 4800, Hitachi, Japan), transmission electron microscopy (TEM, JEM-100CX), and X-ray diffraction (XRD, Philips Xpert Pro) with CuKα radiation generated at 40 kV as a source.

Powders of the pristine SnO_2 and La-doped nanowires were collected by scraping the NWs wafer with a razor blade for the N_2 adsorption/desorption isotherm measurements to estimate the specific surface area of the NWs. The specific surface area of the NWs was calculated by using the Brunauer–Emmett–Teller theory. Pore size distribution and pore volume were obtained method from the adsorption branch of isotherm using the Barrett–Joyner–Halenda (BJH).

The as-obtained SnO_2 NWs were dispersed in a mixture of deionized water (50%) and isopropyl alcohol (50%) via ultrasonication following the drop-coating method to fabricate SnO_2 NWs sensor. The schematic diagram of the sensor fabrication is presented in Fig. 1. A Pt-interdigitated electrode with an area of 800 μm × 1600 μm was fabricated using a conventional photolithographic method with a finger width of 20 μm and a gap size of 20 μm. The interdigitated-electrodes were fabricated by sputtering 10 nm Cr and 200 nm Pt on a layer of a 300 nm thick silicon dioxide (SiO_2) thermally grown on top of the silicon wafer. The slurry containing SnO_2 NWs was dropped on the Pt-interdigitated electrode using a micropipette. The number of droplets and the NWs density were optimized to achieve the best performance of the sensor. After drying the sensor at 120 °C for 5 min, a droplet of aqueous $LaCl_3$ solution (20 μL) was dropped onto the SnO_2 NWs layer to functionalize the SnO_2 NWs surface. The $LaCl_3$ solutions at different concentrations (2, 12, 24, 36, 60, 96 and 120 mM) were used to find the optimal concentration for the best sensor performance. The sensors were heat-treated at 600 °C for 5 h to convert $LaCl_3$ to LaOCl and stabilize the sensor resistance. The gas-sensing characteristics of the LaOCl–SnO_2 NWs and bare SnO_2 NWs sensors were measured under the same experimental conditions. The CO_2 gas concentration was controlled by changing the mixing ratio of dry parent gases and dry synthetic air. A flow-through technique with a constant flow rate of 200 sccm was used, employing a previously described homemade system [24]. The sensors were tested using various toxic gases including 100 ppm CO, 50 ppm C_2H_5OH, 25 ppm H_2, 250 ppm LPG, 25 ppm NH_3 and 5 ppm NO_2 to investigate the selectivity of the sensors. These concentrations were appropriated for various applications, as previously suggested [35]. The gas responses ($S = R_a/R_g$ *or* R_g/R_a) to CO_2, CO, C_2H_5OH, H_2, LPG, NH_3 and NO_2 were measured at 350–450 °C by comparing the sensor resistance in the target gases (R_g) with that in high-purity air (R_a). The dc 2-probe resistance of the sensor was measured using a Kiethley 2700 Digital Multimeter interfaced with a computer.

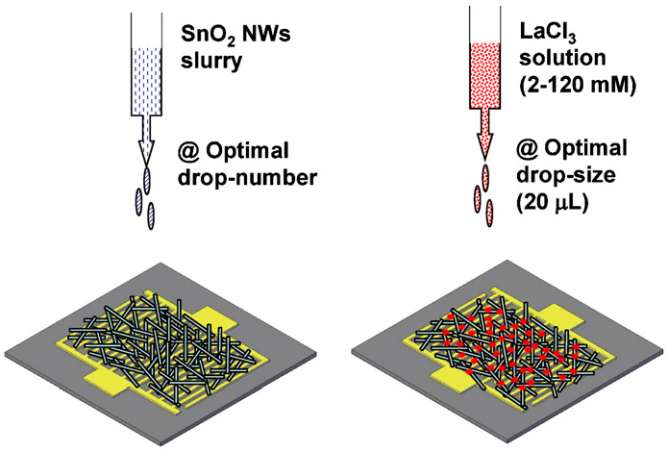

Fig. 1. Schematic fabrication process of LaOCl–SnO_2 NWs sensor.

3. Results and discussion

As-grown SnO_2 NWs and functionalized SnO_2 NWs samples were used for structure and morphology investigations. The functionalized SnO_2 NWs sample was prepared by drop-coating the $LaCl_3$ aqueous solution, followed by heat treatment at 600 °C for 5 h. The morphologies of the as-grown SnO_2 NWs and functionalized SnO_2 NWs recorded by FE-SEM are shown in Fig. 2a and b, respectively. The as-grown SnO_2 NWs have a diameter of 50–150 nm and a length of several micrometers, with relative smooth surface and uniformity along the axis of the wire. By contrast, the functionalized SnO_2 NWs have relatively larger diameters with rough surfaces, which can be attributed to surface modification by LaOCl. Energy dispersive X-ray spectroscopy (EDS) was used to analyze the bare SnO_2 NWs and the functionalized SnO_2 NWs, the results are shown in Fig. 2c and d. Compared with the bare SnO_2 NWs, the composition elements of the functionalized SnO_2 NWs samples include not only Sn and O but also La and Cl. The peaks corresponding to Si come from the Si substrate. The EDS was also performed by mapping on LaOCl–SnO_2 NWs from the SnO_2 NWs samples coated with 9.6 mM $LaCl_3$ solution. The average ratio between Sn and La are 43–49% and 10–17%, respectively. The surface of the bare SnO_2 NWs and functionalized SnO_2 NWs were further characterized via TEM. As depicted in Fig. 2e and f, the bare SnO_2 NWs have clear surfaces, whereas the functionalized SnO_2 NWs have rough surface to be coated with LaOCl lenticular spots. The TEM image also reveals that the surfaces of SnO_2 NWs are mostly coated with the LaOCl spots, although minor amounts of the NWs are bare or coated with the LaOCl in a continuous manner.

Though the oxidation temperature of $LaCl_3$ to LaOCl has been identified, the progressive oxidation of $LaCl_3$ to LaOCl occurs at 500–800 °C [16,17]. However, the oxidation temperatures to

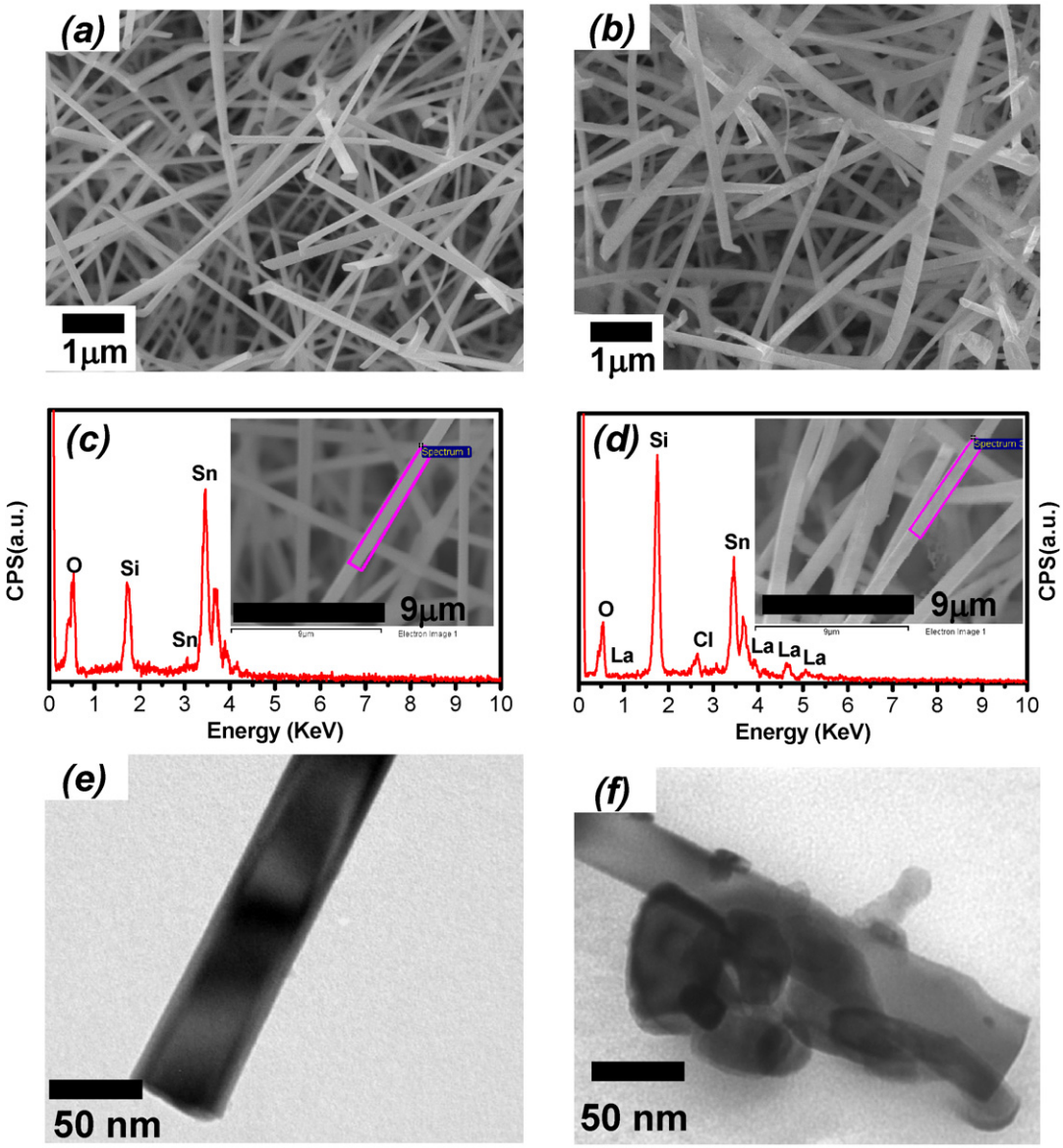

Fig. 2. FE-SEM images, EDS elemental mapping, and TEM images of the bare SnO_2 NWs (a, c, e) and LaOCl–SnO_2 NWs samples (b, d, f).

convert $LaCl_3$ to LaOCl on the surface of SnO_2 NWs still need further study. Therefore, three samples of SnO_2 NWs were functionalized with the $LaCl_3$ solution and subsequently heat-treated at 500, 600, and 700 °C for XRD characterization (Fig. 3). For the bare SnO_2 NWs sample, the sharp diffraction peaks caused by its high crystallinity can be indexed well to the tetragonal rutile structures of SnO_2. The as-obtained XRD patterns of the three samples of LaOCl–SnO_2 NWs were very similar. The typical peaks of SnO_2 and LaOCl phase coexist in the XRD pattern, which is in agreement with previous reports by Marsal and et al. [13] and Kim et al. [12]. The diffraction peaks at 2θ (°) of 26.59°, 33.89°, 37.97°, 38.99°, 54.81°, 57.86°, 61.90°, 64.80° and 66.05° are indexed as the (1 1 0), (1 0 1), (2 0 0), (2 1 1), (2 2 0), (0 0 2), (3 1 0), (1 1 2) and (3 0 1) planes of SnO_2, respectively. These measured diffraction peaks in the 2θ range correspond to the tetragonal structure of SnO_2 with lattice constants $a = 4.73$ Å and $c = 3.18$ Å, which are in good agreement with those in the standard data card (JCPDS Card No. 41-1445). The diffraction peaks at 2θ (°) of 12.81°, 25.17°, 30.68°, 43.96°, 45.22°, 45.96°, 50.61°, 56.67° and 63.87° are indexed as the (0 0 1), (1 0 1), (1 1 0), (2 0 0), (1 0 3), (2 0 1), (1 1 3), (2 1 2), and (2 2 0) planes of LaOCl, respectively. These measured diffraction peaks in the 2θ range correspond to the tetragonal structure of LaOCl with lattice constants $a = 4.12$ Å and $c = 6.88$ Å, which are in good agreement with those in the standard data card (JCPDS Card No. 08-0477). The sharpness of the diffraction peaks suggests that the products (SnO_2 and LaOCL) are well crystallized. The crystallite sizes of SnO_2 and LaOCl were calculated using the Scherrer equation, ($D = K\lambda/\beta\cos\theta$) where D is the grain size, K is a constant (0.94), λ is the wavelength of the X-ray radiation, β is the full width at half maximum, and θ is the angle of diffraction. The crystallite sizes of SnO_2 NWs and LaOCl were calculated as well. The crystallite sizes of SnO_2 in the sample heat-treated at 500, 600 and 700 °C are approximately 22, 25 and 35 nm, respectively, whereas, the crystallite sizes of LaOCl are approximately 24, 26 and 27 nm.

The CO_2 sensing performance of bare SnO_2 NWs and LaOCl–SnO_2 NWs sensors were compared. The LaOCl–SnO_2 NWs sensor was prepared by coating with 9.6 M $LaCl_3$ (optimum value) and heat treatment at 600 °C to ensure the conversion of $LaCl_3$ to LaOCl and stabilize sensor resistance. The sensing transients of the bare SnO_2 NWs and LaOCl–SnO_2 NWs to CO_2 gas concentration

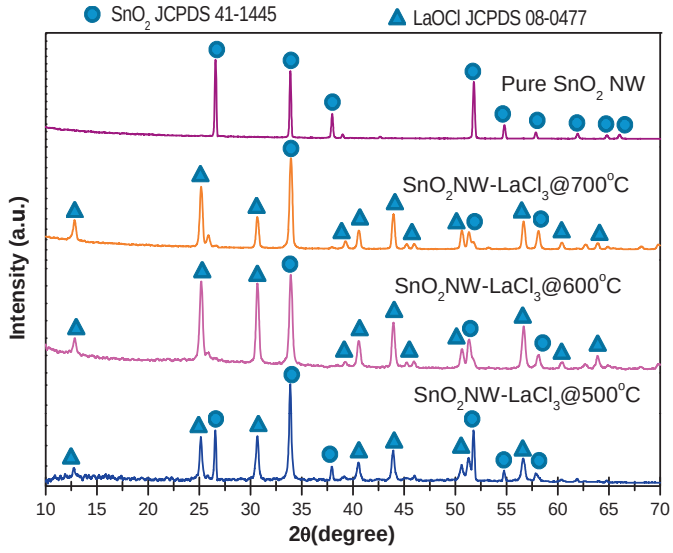

Fig. 3. XRD pattern of bare SnO_2 NWs and $LaCl_3$-functionalized SnO_2 NWs samples heat-treated at 500, 600 and 700 °C.

range of 250–4000 ppm at 350, 400 and 450 °C operating temperatures are shown in Fig. 4. The resistance of the bare SnO_2 and LaOCl–SnO_2 NWs sensors both decreased upon exposure to CO_2 gas. This result suggests that the bare SnO_2 NWs and LaOCl–SnO_2 NWs sensors both exhibited typical n-type gas sensing behaviors, similar with the LaOCl–SnO_2 film sensors [12]. The LaOCl-coated SnO_2 NWs were dominated not by the discrete configuration of p-type LaOCl islands but by the elongated configuration of n-type SnO_2 NWs. As indicated in Fig. 4c, the LaOCl–SnO_2 NWs sensor has good response to CO_2 at concentration as low as 250 ppm and operating temperature as low as 300 °C, whereas, the bare SnO_2 NWs sensor has negligible response to CO_2 gas at such low concentration and operating temperature. Specifically, the CO_2 gas response was calculated using the ratio R_a (resistance in air)/R_g (resistance in CO_2 gas) from the transient response data. The gas responses versus the CO_2 concentration of the bare SnO_2 NWs and LaOCl–SnO_2 NWs sensors are plotted in Fig. 4b and d, respectively. The gas response of the LaOCl–SnO_2 NWs sensor to 4000 ppm CO_2 at 400 °C was about 6.8, whereas that of the bare SnO_2 NWs sensor was about 1.2. This result reveals that the coating of LaOCl noticeably enhances the CO_2 response of the SnO_2 NWs sensor. Result of the present study were compared with those of previous works. The response (R_a/R_g) value to 2000 ppm CO_2 at 400 °C is presented with the previous results in Table 1. The values in present study are higher compared with those previously reported SMO-based gas sensors, indicating that LaOCl–SnO_2 NWs are promising material platforms for the detection of CO_2 gas.

The response and recovery times of a semiconductor sensor are very important issue for practical application. However, previous reports about semiconductor CO_2 gas sensors have not yet investigated these issues [10–17]. In the present work, the 90% response time ($\tau_{resp.90\%}$) for CO_2 exposure and 90% recovery time for air

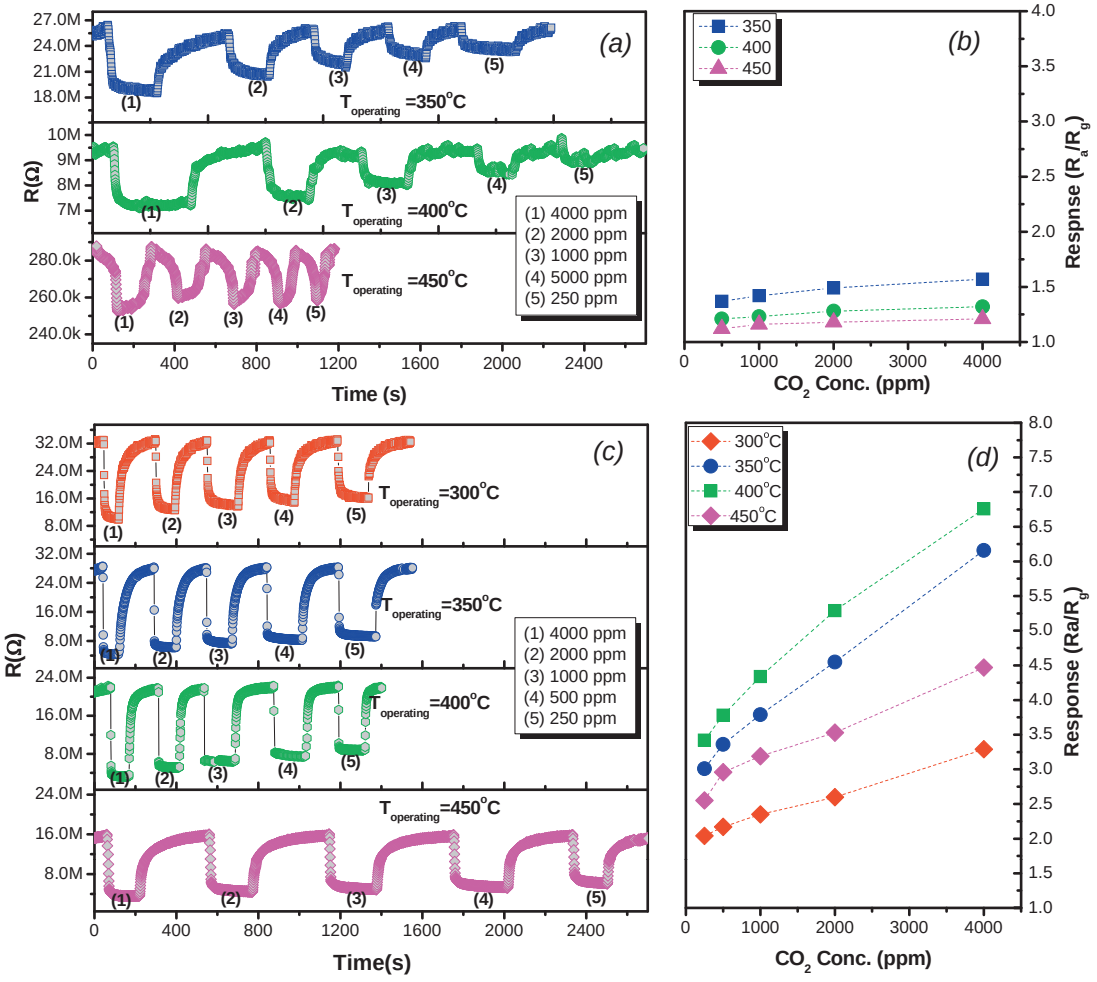

Fig. 4. CO_2 sensing transients and responses at different operating temperatures of the bare SnO_2 NWs (a and b) and LaOCl–SnO_2 NWs (c and d).

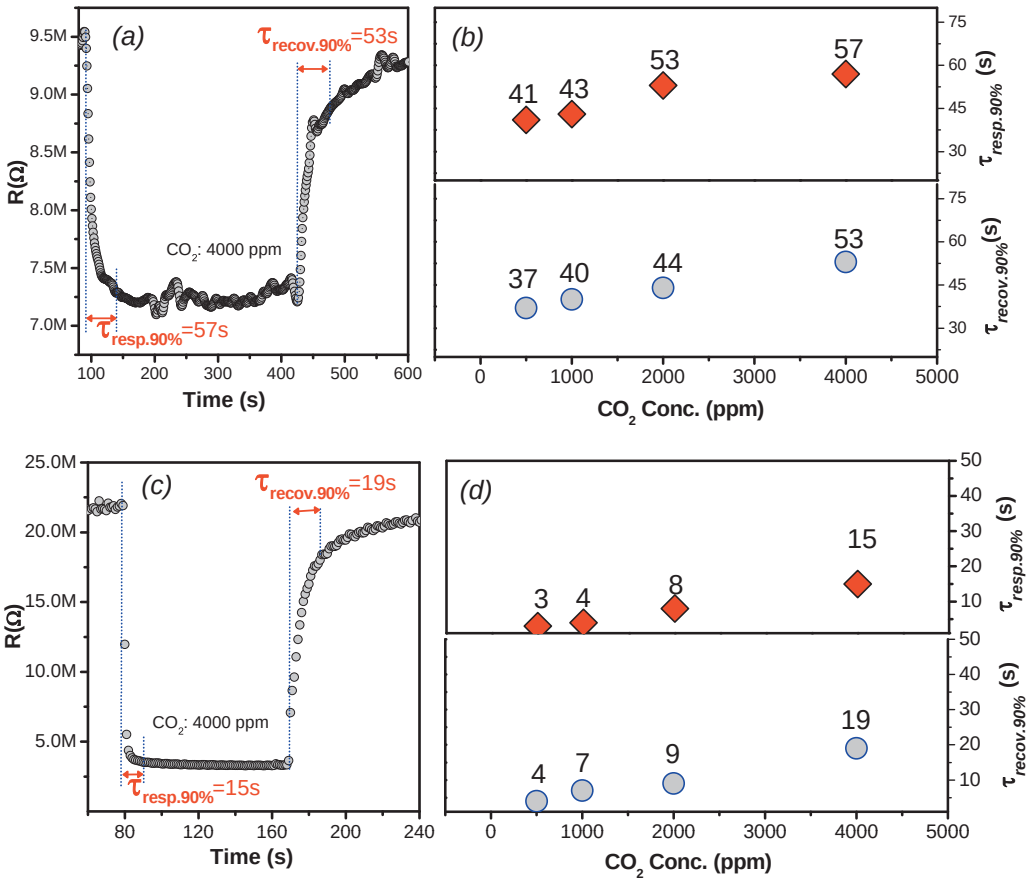

Fig. 5. Typical resistant transient and response–recovery times of the bare SnO_2 NW (a and b) and LaOCl–SnO_2 NWs sensors at 400 °C (c and d).

re-exposure ($\tau_{resp.90\%}$) were calculated from the resistance-time data (Fig. 4a and c) of bare SnO_2 NWs and LaOCl–SnO_2 NWs sensors to compare response–recovery time of the two sensors [21]. The typical dynamic transient resistant of the bare SnO_2 NWs and LaOCl–SnO_2 NWs sensors to 4000 ppm CO_2 at 400 °C are shown in Fig. 5a and c to demonstrate the calculation of response–recovery time. The results are shown in Fig. 5b and d. The $\tau_{resp.90\%}$ values (500–4000 ppm CO_2 at 400 °C) of the bare SnO_2 NWs and the LaOCl–SnO_2 NWs sensors were 41–57 s and 3–20 s, respectively, whereas the $\tau_{recov.90\%}$ values of the bare SnO_2 NWs and the LaOCl–SnO_2 NWs sensors were 37–53 s and 4–19 s. These findings indicate that the LaOCl–SnO_2 NWs sensor does not only have better response but also dynamic response and recovery. The response and recovery times in the present study are much shorter compared with those reported for La_2O_3-doped SnO_2 films, with values approximately 80 s and 90 s, respectively [12]. The 3–20 s response and 4–19 s recovery times for CO_2 sensing is good enough for various applications such as air-quality monitoring, safety regulations and early signal of a volcanic eruption and earthquake.

Table 1
Sensor responses to 2000 ppm CO_2 and operating temperatures of reported studies on semiconductors metal oxides-based CO_2 gas sensors.

Material	Operating temp. (°C)	Sensor response	Ref.
Pt/Ca–SnO_2	270	1.1	[13]
SnO_2–La_2O_3	400	1.4	[11]
SnO_2–LaOCl	425	1.4	[15]
SnO_2–LaOCl	350	1.6	[12]
LaOCl	300	3.4	[16]
CuO–$Cu_xFe_{3-x}O_4$	250	1.9	[14]
SnO_2–LaOCl	400	5.6	This work
(NWs)	350	4.5	This work

Selectivity to CO_2 gas is a serious challenge for SMO-based gas sensors because of the greater chemical stability of CO_2 gas compared with interference toxic gases, such as CO, NO_2, C_2H_3OH, LPG, H_2, and NH_3 in polluted air. The selectivity of SMO-based CO_2 gas sensors, such as La_2O_3-doped SnO_2, LaOCl-doped SnO_2, LaOCl, and CuO [12–16], have not yet been reported. Therefore, the selectivity of LaOCl–SnO_2 NWs sensors at different operating temperatures was examined because operating temperature is a factor that may enhance the selectivity of SMO-based sensors [38]. The gas response of bare SnO_2 NWs and LaOCl–SnO_2 NWs sensors to CO_2 and other gases (CO, C_2H_5OH, H_2, LPG, NO_2, and NH_3) at different operating temperatures are shown in Fig. 6. For the bare SnO_2 NWs, the response value (R_a/R_g) to 4000 ppm CO_2 at 350, 400 and 450 °C were comparable with that to 100 ppm CO, 50 ppm C_2H_5OH, 100 ppm H_2, 250 ppm LPG, 10 ppm NO_2, and 20 ppm NH_3 (Fig. 6a). Therefore, the bare SnO_2 NWs sensor is not capable of selectively detecting CO_2 gas in the presence of CO, C_2H_5OH, H_2, LPG, NO_2, and NH_3 gases. By contrast, the LaOCl–SnO_2 NWs sensor showed increasing selectivity for CO_2 gas. The response values to 4000 ppm CO_2 of this sensor operating at 400 and 450 °C were 6.8 and 6.7, respectively (dark gray bar and light gray bar, Fig. 6b). These values are relatively higher compared with the response values to CO, C_2H_5OH, H_2, LPG, NO_2, and NH_3 (1.4–2.7 at 400 °C and 1.1–1.7 at 450 °C, Fig. 6b). The sensor operating at 350 °C demonstrated quite a good response to C_2H_5OH and H_2 gases (Fig. 6b). Therefore, its selectivity to CO_2 gas is quite poor.

LaOCl plays an important role in enhancing the performance of SnO_2 NWs sensor to CO_2 gas. Previous studies reported that the density of catalyst coating on the surface of NWs may affect the sensing performance of functionalized NWs sensors [19–21]. The direct control of the density of LaOCl functionalization can

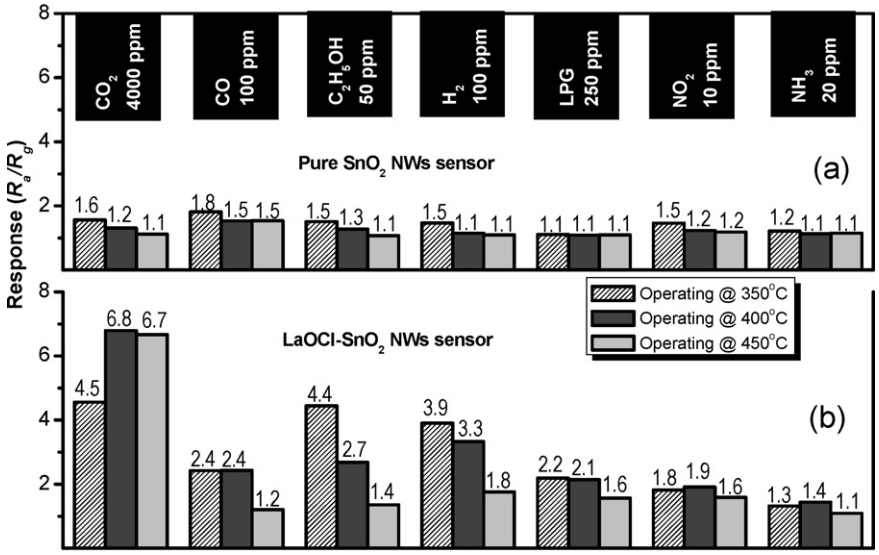

Fig. 6. Gas response of (a) the bare SnO_2 NWs and (b) LaOCl–SnO_2 NWs sensors to CO, C_2H_5OH, H_2, LPG, NO_2, and NH_3.

be conducted by varying the concentration of the $LaCL_3$ aqueous solution from 2 to 120 mM. The SnO_2 NWs sensors functionalized with these solutions and heat-treated at 600 °C were measured at different operating temperatures (300–450 °C) and CO_2 concentration range of 250–4000 ppm. The obtained results are shown in Figs. S1 to S4 (Supplementary). The as-obtained responses to 4000 ppm CO_2 at different operating temperatures as a function of the concentration of $LaCl_3$ aqueous solution are shown in Fig. 7a. The LaOCl–SnO_2 NWs sensor that used 90 mM $LaCl_3$ solution obtained the highest response at different operating temperatures. The responses of the LaOCl–SnO_2 NWs sensors as a function of CO_2 concentration at 400 °C operating temperature are presented in Fig. 7b. The variation in sensor response to CO_2 gas by varying the $LaCl_3$ solution concentration increases with increasing CO_2 gas concentration. The responses to 250–4000 ppm CO_2 gas of the best and worst LaOCl–SnO_2 NWs sensors are in the range of 3.6–6.8 and 1.4–2.1, respectively. This result suggests that optimization of the functionalizing process should be conducted to develop the LaOCl–SnO_2 NWs sensor. The optimal concentration of the $LaCl_3$ solution in the present study cannot be used for other kinds of NWs sensors, such as on-chip grown [25,26], Au screen-printed electrode [21], and dielectrophoretically assembled NWs sensors [36]. The optimum concentration of the coating solution should be found for particular cases.

The good performance of LaOCl–SnO_2 NWs sensors has so far remained unclear, extensive studies need to be conducted to obtain a plausible explanation. First, the specific surface areas of the materials influence the gas sensor performance. Thus, the specific area of SnO_2 and LaOCl–SnO_2 NWs were estimated for comparison. The specific surface area and pore volume of pristine SnO_2 NWs were 4.00 $m^2\,g^{-1}$, and 0.044 $cm^3\,g^{-1}$, respectively, whereas those of LaOCl–SnO_2 NWs were 2.20 $m^2\,g^{-1}$ and 0.0065 $cm^3\,g^{-1}$, respectively. (Figs. S5 and S6, Supplementary). The low values of specific surface area and pore volume were due to the non-porous structure of the NWs [37]. This result is consistent with the TEM analysis, where the NWs prepared by seed catalyst chemical vapor deposition method grew single crystal NWs. The lower specific surface area of LaOCl–SnO_2 NWs compared with that of bare SnO_2 NWs was possibly due to the aggregation of NWs after functionalization. Alternatively, the enhancement of the CO_2 sensing performance of the LaOCl-coated SnO_2 NWs sensor was speculated in the present study based on two concepts. The first concept is "*electronic mechanism*", in which the LaOCl–SnO_2 NWs have caused the extension

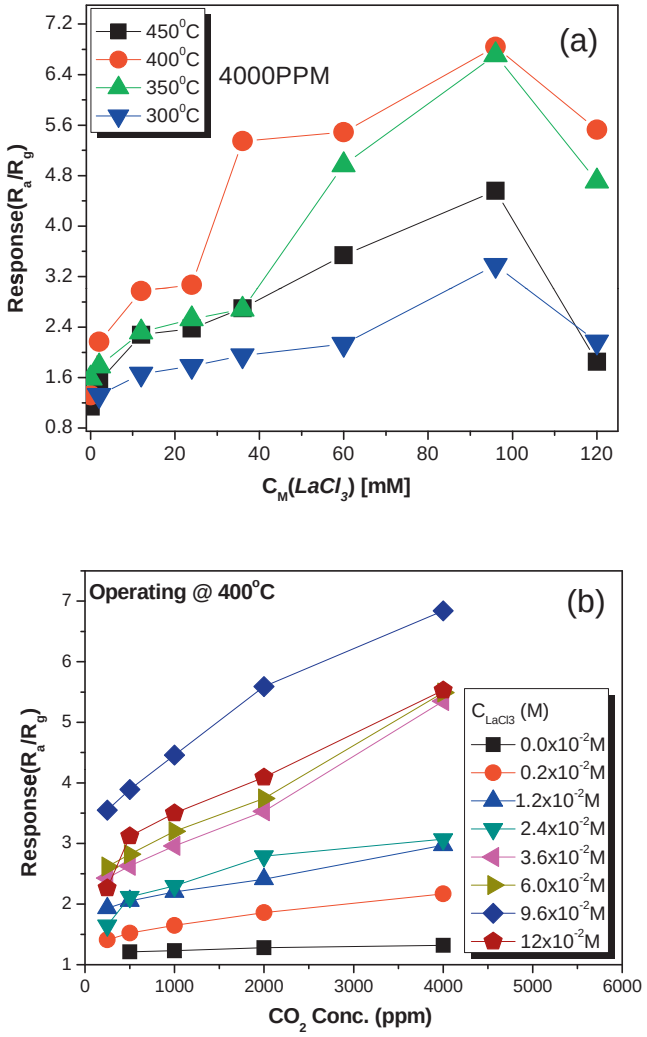

Fig. 7. (a) Gas response to 4000 ppm CO_2 versus $LaCl_3$ coating solution concentration at different operating temperatures and (b) the response of LaOCl–SnO_2 NWs sensors as a function of CO_2 gas concentration.

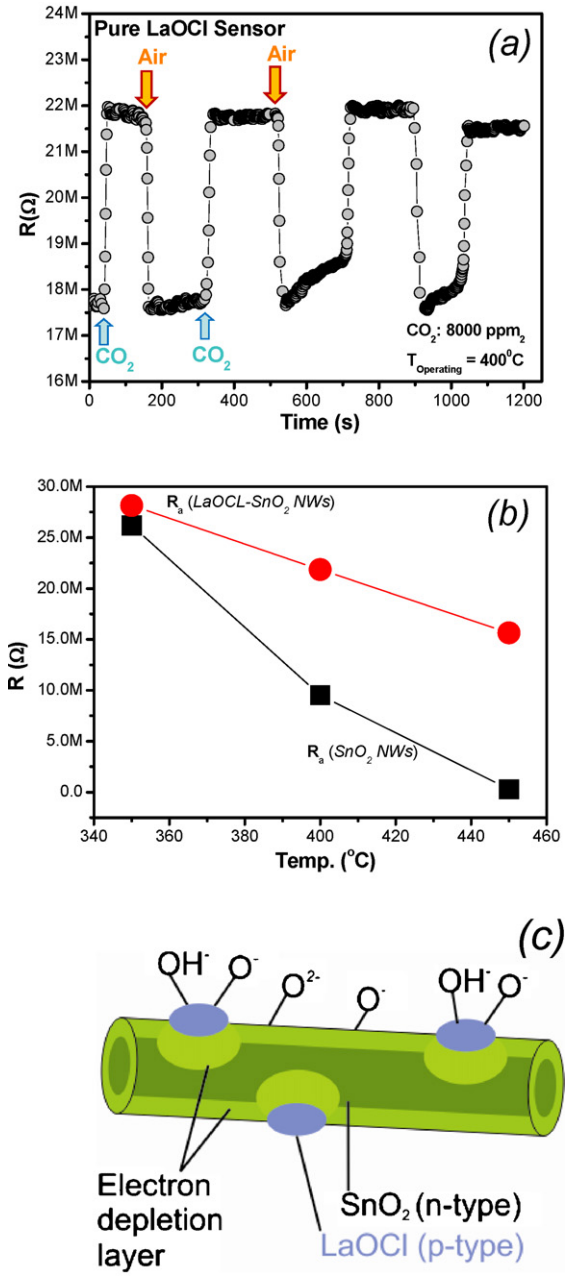

Fig. 8. (a) The p-type sensing behavior of bare LaOCl materials, (b) resistance versus temperature of bare SnO_2 NWs and LaOCl–SnO_2 NWs sensors and (c) extension of the depletion layer of SnO_2 NWs functionalized with LaOCl.

of the electronic depletion layer due to the formation of p–n junction between the p-type LaOCl and n-type SnO_2 NWs [34,39]. The p-type sensing behavior of LaOCl has been confirmed by previous works [13,17] and the current data, which exhibited the resistance of pure LaOCl sensor increased upon expose to CO_2 gas as shown in Fig. 8a. The formation of the p–n junction resulted that the R_a of LaOCl–SnO_2 NWs sensors is higher than that of the bare SnO_2 NWs sensors as indicated in Fig. 8b. Thus, the increase of R_a/R_g (response) can be aslo explained by the increase of R_a due to the creation of a resistive p–n junction between LaOCl and SnO_2 NWs. As shown in Fig. 6, the response of LaOCl–SnO_2 sensor to all the tested gases are higher compared with that of the bare SnO_2 sensor. However, the only response of the LaOCl–SnO_2 sensor to CO_2 gas is much higher than that of the bare SnO_2 sensor. This findings can be explained by the second concept of the so-called "*chemical mechanism*", in which LaOCl is a favorable catalyst for CO_2 gas [39–41]. Usually, only O^- and O^{2-} are adsorbed on the surface of metal oxides at elevated temperature. However, in cases of LaOCl, beside of the adsorption of O^- and O^{2-}, the OH^- is also adsorbed surface of the LaOCl at elevated temperature [40,41], which is confirmed by our FTIR measurements conducted in the present study (Fig. S7, Supplementary). When the LaOCl–SnO_2 NWs sensor is exposed to CO_2 gas, the CO_2 molecules can chemically react with these adsorbed species to form polydentate carbonates and hydroxycarbonates [40], resulting in the phase transformation of LaOCl, disruption of the p–n junction and, consequently, decreased resistance of the LaOCl–SnO_2 NWs sensor. The reaction of CO_2 with OH^- and O^{2-} on the surface of LaOCl forming the carbonates and hydroxycarbonates has been confirmed through experimental and simulated investigations [41]. The presence of humidity influences CO_2 response [12,13]. However, this supposition has not been investigated in the present study. Above explained the CO_2 senisng mechanism of LaOCl–SnO_2 NWs sensor is not completely clear. However, the above speculation is to stimulate further investigation, that may lead to the development of multi-sensors based on SnO_2 NWs for environmental monitoring.

4. Conclusion

In the present study, a novel LaOCl–SnO_2 NWs sensor with good sensitivity, selectivity, and favorable response–recovery in detecting CO_2 gas was developed. This sensing material can solve the problem of conventional SMO sensing materials that could hardly detect CO_2 gas because of the chemical stability of the gas. The functionalization with LaOCl can increase the response of SnO_2 NWs sensor to 4000 ppm CO_2 gas by a factor about 6. Therefore, the selectivity to CO_2 is enhanced compared with various toxic gases, such as CO, C_2H_5OH, H_2, LPG, NO_2, and NH_3. The response and recovery times of LaOCl–SnO_2 NWs sensors are shorter compared with those of the bare SnO_2 NWs sensor. The enhanced CO_2 sensing performance is attributed to the extension of the electron depletion layer by the formation of p–n junctions and the favorable catalyst effect of LaOCl to CO_2 gas. The functionalization of n-type SnO_2 NWs with p-type active catalyst provides a facile and powerful method to control the sensitivity and the selectivity of NWs sensors for environmental monitoring.

Acknowledgments

This work was financially supported by the Vietnam's National Foundation for Science and Technology Development (Nafosted, Code: 104.05.13.09) and by the application-oriented basic research program (2009–2012, Code: 05/09/HĐ-DTĐL).

Appendix A. Supplementary data

Supplementary data associated with this article can be found, in the online version, at doi:10.1016/j.talanta.2011.10.024.

References

[1] G. Eranna, B.C. Joshi, D.P. Runthala, R.P. Gupta, Crit. Rev. Solid State Mater. Sci. 29 (2004) 11–188.
[2] S. Akbar, P. Dutta, C. Lee, Int. J. Appl. Ceram. Technol. 3 (2006) 302–311.
[3] S.G.D. Santos-Alves, R.F. Patier, Sens. Actuators B 59 (1999) 69–74.
[4] F. Charpentier, B. Bureau, J. Troles, C.B-. Pledel, K.M.-L. Pierres, F. Smektala, J.-L. Adam, Opt. Mater. 31 (2009) 496–500.
[5] T. Goto, G. He, T. Narushima, Y. Iguchi, Solid State Ionics 156 (2003) 329–336.
[6] T. Ishihara, K. Komentani, Y. Miyuhara, Y. Takita, Sens. Actuators B 13 (1993) 470–472.
[8] C. Lim, W. Wang, S. Yang, K. Lee, Sens. Actuators B 154 (2011) 9–16.
[9] Y. Liu, Y. Tang, N.N. Barashkov, I.S. Irgibeva, J.W.Y. Lam, R. Hu, D. Birimzhanova, Y. Yu, B.Z. Tang, J. Am. Chem. Soc. 132 (2010) 13951–13955.

[10] P. Samarasekara, N.U.S. Yapa, N.T.R.N. Kumara, M.V.K. Perera, Bull. Mater. Sci. 30 (2007) 113–116.
[11] N. Mizuno, T. Yoshioka, K. Kato, M. Iwamoto, Sens. Actuators B 13–14 (1993) 473–475.
[12] D.H. Kim, J.Y. Yoon, H.C. Park, K.H. Kim, Sens. Actuators B 62 (2000) 61–66.
[13] A. Marsal, A. Cornet, J.R. Morante, Sens. Actuators B 94 (2003) 324–329.
[14] U. Hoefer, G. Kuhner, W. Schweizer, G. Sulz, K. Steiner, Sens. Actuators B 22 (1994) 115–119.
[15] H.A. Diagne, M. Lumbreras, Sens. Actuators B 3957 (2001) 1–8.
[16] A. Marsal, G. Dezanneau, A. Cornet, J.R. Morante, Sens. Actuators B 95 (2003) 266–270.
[17] A. Marsal, E. Rossinyol, F. Bimbela, C. Tellez, J. Coronas, A. Cornet, J.R. Morante, Sens. Actuators B 109 (2005) 38–43.
[18] A. Kolmakov, M. Moskovits, Annu. Rev. Mater. Res. 34 (2004) 150–180 (review).
[19] A. Kolmakov, D.O. Klenov, Y. Lilach, S. Stemmer, M. Moskovits, Nano Lett. 5 (2005) 667–673.
[20] H. Li, J. XU, Y. Zhu, X. Chen, Q. Xiang, Talanta 82 (2010) 458–463.
[21] N.V. Hieu, H.-R. Kim, B.-K. Ju, J.-H. Lee, Sens. Actuators B 133 (2008) 228–234.
[22] X.Y. Xue, Y.J. Chen, Y.G. Liu, S.L. Shi, Y.G. Wang, T.H. Wang, Appl. Phys. Lett. 88 (2006) 201907–201913.
[23] I.-S. Hwang, S.-J. Kim, J.-K. Choi, J. Choi, H. Ji, G.-T. Kim, G. Cao, J.-H. Lee, Sens. Actuators B 148 (2010) 595–600.
[24] L.V. Thong, L.T.N. Loan, N.V. Hieu, Sens. Actuators B 112 (2010) 112–119.
[25] Y.-J. Choi, I.-S. Hwang, J.-G. Park, K.J. Choi, J.-H. Park, J.-H. Lee, Nanotechnology 19 (2008) 095508–0905512.
[26] L.V. Thong, N.D. Hoa, D.T.T. Le, D.T. Viet, P.D. Tam, A.T. -Le, N.V. Hieu, Sens. Actuators B 146 (2010) 361–367.
[27] S.H. Lee, G. Jo, W. Park, S. Lee, Y.-S. Kim, B.K. Cho, T. Lee, W.B. Kim, ACS Nano 4 (2010) 1829–1836.
[28] J.D. Prades, R.J. Diaz, F.H. Ramirez, S. Barth, A. Cirera, A.R. Rodriguez, S. Mathur, J.R. Morante, Appl. Phys. Lett. 93 (2008) 123110–123113.
[29] A. Kolmakov, X. Chen, M. Moskovits, J. Nanosci. Nanotech. 8 (2008) 111–121.
[30] G.F. Fine, L.M. Cavanagh, A. Afonja, R. Binions, Sensors 10 (2010) 5469–5502.
[31] J.M. Lee, J. Park, S. Kim, S. Kim, E. Lee, S.-J. Kim, W. Lee, Int. J. Hydrogen Energy 35 (2010) 12568–12573.
[32] L.H. Qian, K. Wang, Y. Li, H.T. Fang, Q.H. Lu, X.L. Ma, Mater. Chem. Phys. 100 (2006) 82–84.
[33] I.-S. Hwang, J.-K. Choi, S.-J. Kim, K.-Y. Dong, J.-H. Kwon, B.-K. Ju, J.-H. Lee, Sens. Actuators B 142 (2009) 105–110.
[34] B-.Y. Wei, M-.Ch. Hsu, P-.G. Su, H.-M. Lin, R.-J. Wu, H.-J. Lai, Sens. Actuators B 101 (2004) 81–89.
[35] N. Yamazoe, Sens. Actuators B 108 (2005) 2–14.
[36] W.J. Liu, J. Zhang, L.J. Wana, K.W. Jiang, B.R. Tao, H.L. Li, W.L. Gong, X.D. Tang, Sens. Actuators B 133 (2008) 664–670.
[37] H. Kim, J. Cho, J. Mater. Chem. 18 (2008) 771–775.
[38] A. Fort, M. Gregorkiewitz, N. Machetti, S. Rocchi, B. Serrano, L. Tondi, N. Ulivieri, V. Vignoli, G. Faglia, E. Comini, Thin Solid Films 418 (2002) 2–8.
[39] C. Marichy, N. Donato, M.G. Willinger, M. Latino, D. Karpinsky, S.-H. Yu, G. Neri, Pinna, Adv. Funct. Mater. 21 (2011) 658–666.
[40] A. Marsal, M.A. Centenob, J.A. Odriozolab, A. Cornet, J.R. Morante, Sens. Actuators B 108 (2005) 484–489.
[41] O.V. Manoilova, S.G. Podkolzin, B. Tope, J. Lercher, E.E. Stangland, J.-M. Goupil, B.M. Weckhuysen, J. Phys. Chem. 108 (2004) 15770–21578.